ISSN 1028-334X, Doklady Earth Sciences, 2025, Vol. 520:45. © Pleiades Publishing, Ltd., 2025.

SEISMOLOGY

Two Types of Seismic Activity Prior to the 2006 Eruption of Augustine Volcano in Alaska

E. M. Grekov[a,b,*], Corresponding Member of the RAS P. N. Shebalin[a], and V. B. Smirnov[b,c]

[a] *Institute of Earthquake Prediction Theory and Mathematical Geophysics, Russian Academy of Sciences, Moscow, Russia*

[b] *Faculty of Physics, Moscow State University, Moscow, Russia*

[c] *Schmidt Institute of Physics of the Earth, Russian Academy of Sciences, Moscow, Russia*

**e-mail: grekov.em16@physics.msu.ru*

Received November 2, 2024; revised December 4, 2024; accepted December 5, 2024

Abstract—The changes in volcanic seismicity regimes by the example of the 2006 eruption of Augustine Volcano in Alaska are analyzed. During the long-term volcanic swarm preceding the eruption, two processes with different seismicity regimes were identified. The first can be associated with general radial deformations caused by an increase in pressure in the underground magma chamber; such a regime has a high value of the slope of the magnitude—frequency distribution and a low degree of clustering. The second process can presumably be associated with an dike intrusion and local destruction of rocks under the pressure of the dike. This process has a slope parameter of the magnitude—frequency distribution close to one and shows a high level of clustering before the most significant events, which are followed by quiescence.

Keywords: volcanic seismicity, grouping of seismicity, nearest neighbor method, volcanic swarms

DOI: 10.1134/S1028334X24605273

INTRODUCTION

This work focuses on the study of endogenous and exogenous factors in volcanic seismicity, particularly volcanic swarms. From this point of view, earthquakes of any nature can be divided into two groups. The first group includes background events that occur independently of one another. These events are caused by external influences, such as the movement of tectonic plates. The second group consists of clustered events, earthquakes that are statistically related with other earthquakes and are hypothetically initiated by them. Such events are determined by endogenous factors, i.e., the internal state of the system [1]. Studying the grouping of events allows the recognition of statistical relationships among earthquakes and clustering events, e.g., series of aftershocks following major events. It is interesting to analyze how volcanic seismicity behaves from this perspective, since it is likely to have a different mechanism of initiation compared to tectonic seismicity. Thus, this may shed light on both the nature of volcanic swarms and the mechanism of earthquake triggering in general. Attempts to conduct such a study have already been made. For example, an analysis of distributions of time intervals among events was used in [2] to study the processes of dike intrusions at the Etna and Vesuvius volcanoes. These processes were found to differ significantly from tectonic seismicity processes.

DATA

This work focuses on volcanic swarms observed prior to the 2006 eruption of Augustine Volcano in Alaska, which occurred from January 11, 2006, to March 16, 2006. At the onset of the eruption, from January 11, 2006, to January 28, 2006, explosive volcanic activity was observed, and after January 28, 2006, the continuous eruption phase (on-going ash ejection) began, which then smoothly changed to the effusive phase (lava outflow) during the first week of February; the eruption was terminated by an extrusive phase starting on March 3, 2006 [3]. Two swarms of events were observed prior to the eruption: a long swarm (from April 30, 2005, to January 10, 2006) and a short swarm (for 13 hours before January 11, 2006) [4].

For this analysis, we use the data from the Alaska Volcano Observatory (AVO) earthquake catalog [5], which covers the period from 1989 to 2018. During this time, only one eruption occurred at the volcano. The events of the long and short swarms under consideration are shown in Fig. 1. The long swarm is divided into two phases. The second phase approximately corresponds to the onset of magma intrusion through a dike [6]. November 21, 2005, was chosen as the separation date based on homogeneity of the seismicity, while according to surface deformation measurement, magma intrusion started on November 17, 2005. In this study, we consider events occurring directly beneath the volcanic edifice, within an area bounded

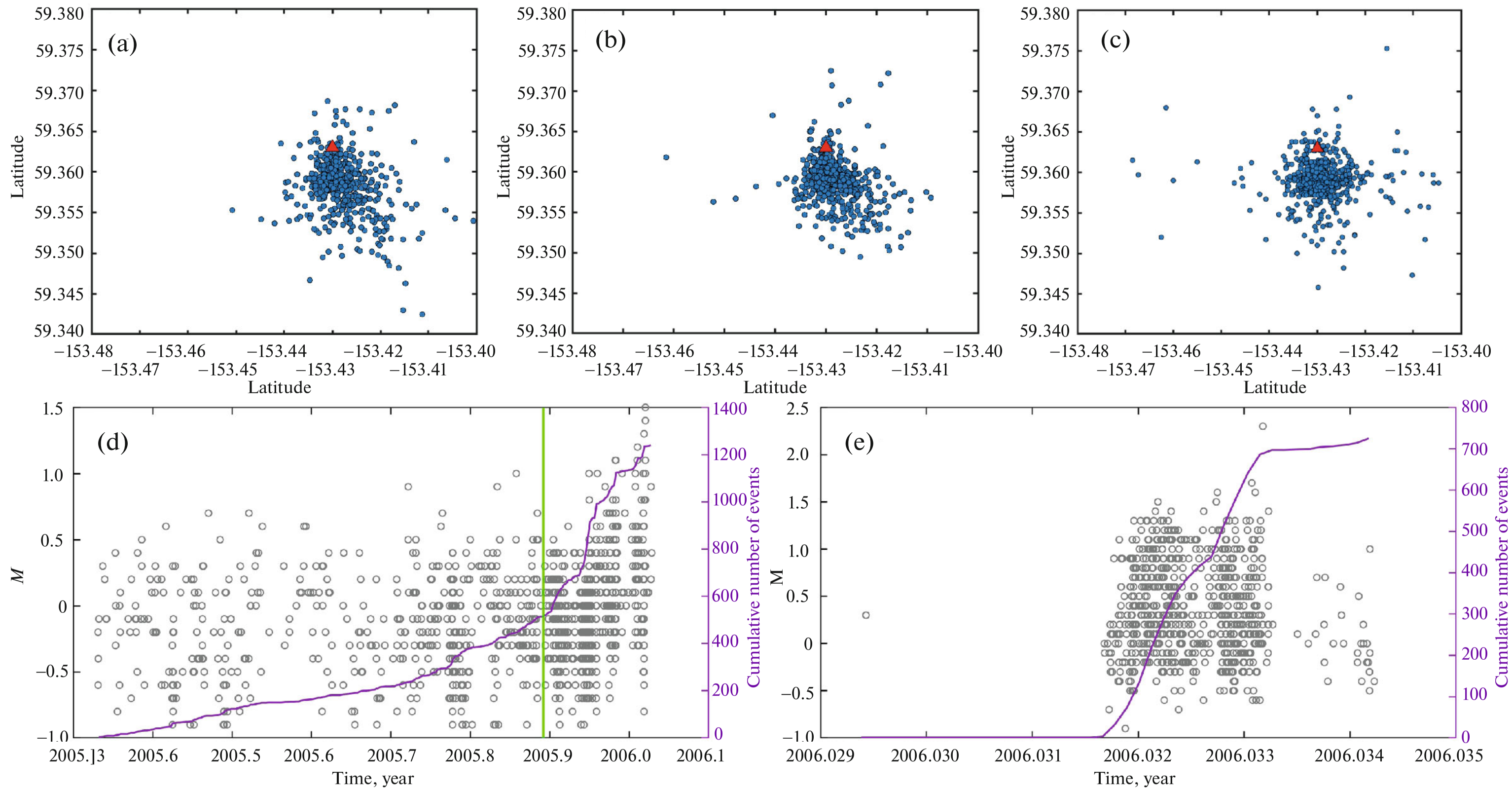

Fig. 1. Distribution of events with magnitudes above the completeness threshold Mc = 0.1 in space and time for the study region. (a) Spatial distribution for the first phase of the long swarm (before November 21, 2005), (b) for the second phase of the long swarm (after November 21, 2005), and (c) for the short swarm. Blue circles designate earthquake epicenters; the red triangle denotes the approximate site of the 2006 eruption of the Augustine Volcano. The time distribution of events: (d) long swarm, (e) short swarm. Circles show the occurrence times of earthquakes; the purple line represents the cumulative number of events. The vertical line shows the date of November 21, 2005, dividing the two phases of the long swarm.

Table 1. Parameters of sequences of seismic events during the three intervals considered

Phase	Interval	Number of events	b	k	k_1	k_1^1	$M_{\max}$	$\bar{M}$
First phase of the long swarm	Apr. 30, 2005–Nov. 21, 2005	145	1.822	0.90	0.87	0.94	1	0.2766
Second phase of the long swarm	Nov. 21, 2005–Jan. 10, 2006	296	1.456	0.64	0.72	0.85	1.5	0.3412
Short swarm	Jan. 10, 2006–Jan. 12, 2006	510	0.869	0.99	–	0.98	2.3	0.5998

by longitude –153.48 to –153.40 and latitude 59.34 to 59.38. Thus, we analyzed three time intervals within these boundaries: the two phases of the long swarm and the period of the short swarm.

METHODS

The grouping of seismic events is analyzed by the nearest neighbor method proposed by Zaliapin [7, 8]. This method makes it possible to identify unambiguously the relationships between seismic events. For this purpose, we use the proximity function introduced in [9]:

$$\eta_{ij} = \begin{cases} t_{ij} r_{ij}^{d_f} 10^{-bm_i}, & t_{ij} > 0 \\ +\infty, & t_{ij} \le 0\,, \end{cases} \tag{1}$$

where t_{ij} is the time interval between events i and j; r_{ij} is the spatial distance between their epicenters, m_i is the magnitude of the event i; b is the parameter of the Gutenberg–Richter law [10]; and d_f is the fractal dimension of the distribution of earthquake epicenters. In fact, this function determines the probability of a random occurrence of a second event at a given distance in space and time from the first event on the assumption that all events are independent. The smaller the value of the function, the less likely such a pair of events occurs randomly, and the more likely they are connected. Clustered and independent events can be determined by the threshold value of η^0: the events are clustered if for a pair of events $\eta_{ij} \le \eta^0$.

For an arbitrary event, we find its "nearest neighbor" preceding in time by the minimum of function (1). The threshold η^0 is calculated by the distribution of the values of function (1) calculated for each event and its respective nearest neighbor. These distributions are usually bimodal [8, 11], and the threshold value can be found using the method from [8] where the distribution is approximated by the sum of two lognormal distributions or by the method from [11] where the distribution for independent events is modeled by random shuffling of event times relative to the epicenter coordinates and magnitude, while the distribution for connected events is modeled by the difference between the actual distribution and the obtained distribution with factor k that provides the best match of two curves on the right side. In both methods, the threshold η^0 is estimated by balancing the proportions of errors when independent pairs of events were assigned to clustered events and vice versa.

The cases of unimodal distributions can also occur [12]. Unimodal distributions may correspond to the cases when the catalog has a small proportion of clustered events and to the cases when the density of independent events is very high. In the second case, the mode of distribution associated with independent events shifts towards smaller values, and the two distributions merge into a unimodal shape. Using the method in [11], threshold η^0 can be determined and independent and clustered events can be distinguished in such cases [12]. We also use this method in our work. It is described in detail in [13]. However, when the quantity of data is small, the results of modeling the distribution for independent events by shuffling their event times can vary significantly; therefore, 20 shuffling procedures are performed, and the best option is selected in terms of the approximation of the right slope of the actual distribution.

For visual control of determining the threshold η^0, it is convenient to use 2D representation of function (1) [8] in a double logarithmic scale. Function (1) is separated into two factors: rescaled time $T = t_{ij} 10^{-0.5bm_i}$ and rescaled distance $R = r_{ij}^{d_f} 10^{-0.5bm_i}$. The 2D distribution of the T and R values for the pairs of all events and their respective "nearest neighbors" usually demonstrates a good separation between independent and clustered events. The threshold η^0 is represented on the diagram as a straight line defined by the equation $\log T + \log R = \log \eta^0$. The alternative value of the threshold can be determined on the diagram by the line $\log T + \log R = \log \eta^1$ which visually best separates the two groups of values.

To analyze the data, we need to determine the completeness magnitude Mc in the catalog. The MAXC (Maximum Curvature) method [14] was used to do that. For all time intervals, we obtained consistent estimates of Mc = 0.1. The parameters b and d_f are present in (1). To estimate parameter b, we use Bender's method [15]. The fractal dimension d_f was calculated using the Grassberger–Procaccia algorithm [16] once for all events in the catalog, and one value of $d_f = 1.93$ is used for all intervals.

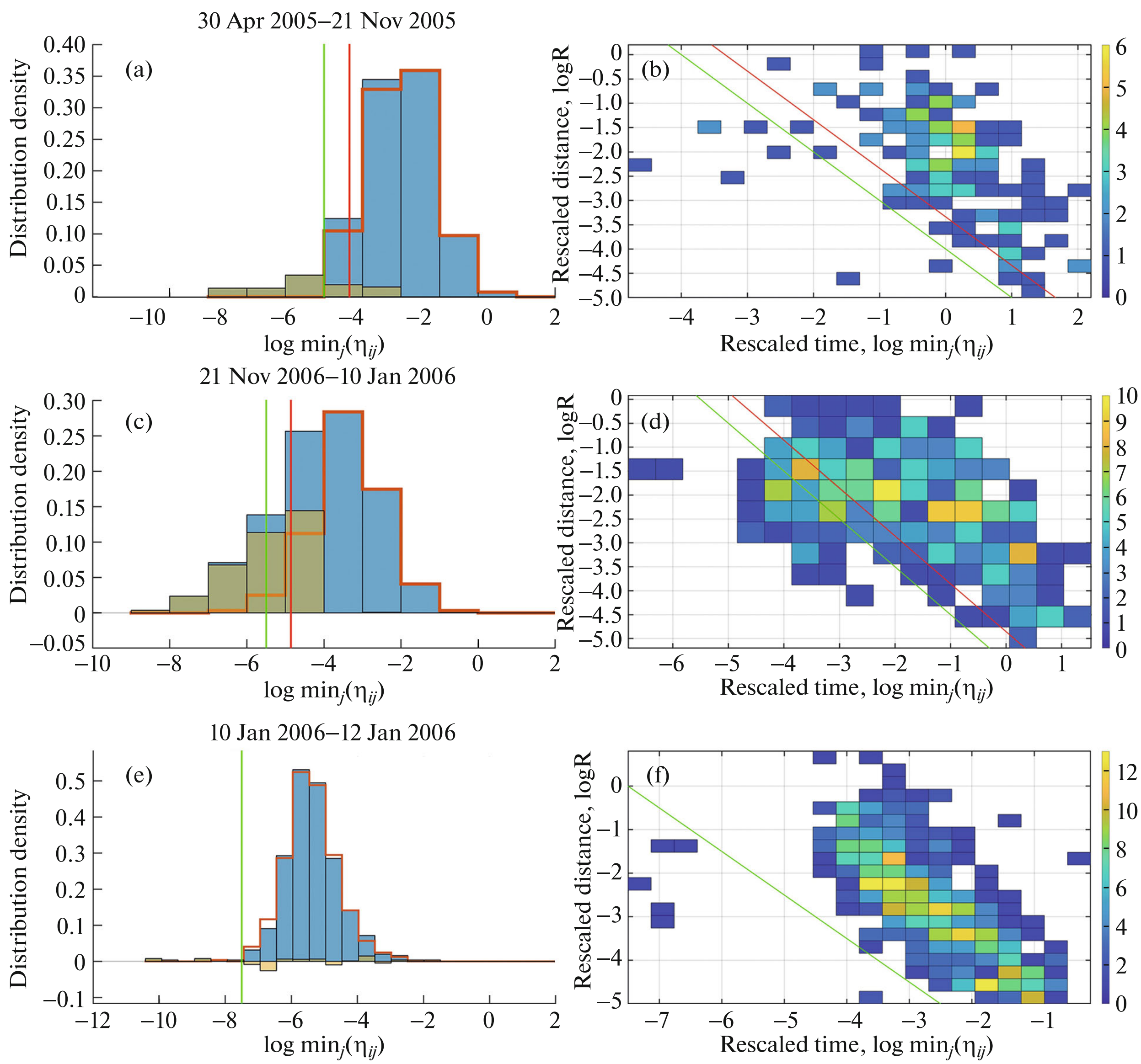

Fig. 2. Analysis of grouping of seismic events. Three intervals are considered: the two phases of the long swarm (a, b and c, d), and the short swarm (e, f). One-dimensional distributions of function (1) for each event relative to its "nearest neighbor," and the results of threshold η^0 determination are presented on the left (a, c, e). Blue bars designate the actual histograms; the red outline marks the histogram of the shuffled catalog with a k factor that provides the best match of the distributions on the right side; and the yellow bars denote the difference between the two histograms, modeling the distribution of clustered events. The vertical line indicates the determined value of threshold η^0. Joint unnormalized distributions of rescaled distances R and times T are provided on the right (b, d, f). Red lines designate the threshold η^0, and green lines, the threshold η^1.

The goal of this work is to compare the degree of grouping of seismic events in the different stages of preparation for the 2006 eruption of Augustine Volcano. Using the method described for determination of threshold η^0, the degree of grouping is estimated by the k factor, which determines the proportion of independent events in the total number. Another approach to determine the degree of grouping is to calculate the proportion of events for which the value of function (1) with the "nearest neighbor" exceeds the threshold η^0. We denote this parameter as k_1. The values of k_1 and k may differ slightly, as k is independent of the threshold η^0, while k_1 is dependent. The grouping of events into those that are independent and those connected by threshold η^0 implies errors in assigning one-type events to another type and vice versa. In this case it is not the number but the proportions of errors on either side estimated by the distribution that are balanced. Therefore, as a result, factors k_1 and k should align closely only when $k = 0.5$. With the alternative, visually determined threshold η^1, k cannot be calculated, but the proportion of independent events based on the threshold η^1 can still be calculated. We denote this value as k_1^1.

RESULTS

Figure 2 shows the results of grouping the events into independent events and those connected for the three time intervals analyzed; Table 1 provides the corresponding values and estimates of the parameter. Table 1 also presents the magnitude $M_{\max}$ of the largest event in the given interval and the average magnitude $\bar{M}$.

For all three intervals, the one-dimensional distributions are unimodal. Nevertheless, as a result of the analysis, both variants, one-dimensional (Figs. 2a, 2c, 2e) and two-dimensional (Figs. 2b, 2d, 2f), demonstrate a predominant proportion of independent events in the first phase of the long swarm and during the short swarm. In contrast, in the second phase of the long swarm, which corresponds to dike intrusion [6], a relatively high proportion of clustered events is observed. For the short swarm events (Fig. 2e), the threshold η^0 value cannot be determined, since after shuffling the catalog, the distribution of the values of function (1) closely match the original distribution; thereby almost all events can be considered independent.

We studied the second phase of the long swarm, the period of intrusion, in more detail (Figs. 2c, 2d). Despite the relatively high proportion of clustered events, even the two-dimensional distribution (Fig. 2d) does not clearly distinguish between the two types of events as in [8], which more likely resembles the case of randomization of event times in the catalog relative to the epicenter coordinates and magnitude. It is possible that the study area is so small that the errors in determining the coordinates lead to a distorted distribution, hiding the grouping. This is indirectly implied by the fractal dimension value, which is close to two. Therefore, as an additional variant of function (1), we use the proximity function without distances between epicenters:

$$\eta_{ij}^1 = \begin{cases} t_{ij}10^{-cm_i}, & t_{ij} > 0 \\ +\infty, & t_{ij} \le 0, \end{cases} \qquad (2)$$

where c is a coefficient. At $c = b/2$, expression (2) corresponds to the rescaled time T. Then we used the value of $c = 0.3$ [17, 11]. However, the results differ little if we use $c = b/2$. The distribution of the values of function (2) for events relative to "nearest neighbors" and its decomposition into the distribution for the independent and clustered events are shown in Fig. 3. The distribution has a clear bimodal shape. In this case, the procedure of shuffling is useless; therefore, for decomposition this procedure was changed to simple redetermination of the nearest neighbors after the removal of a priori connected events from the catalog. Similar to [11], a priori connected events are considered events for which the proximity function value is below the threshold determined as the half-height of the right maximum on the left slope (Fig. 3).

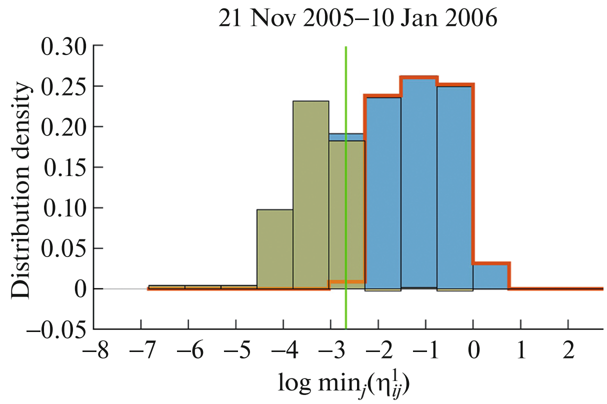

Fig. 3. Analysis of grouping of seismic events using the proximity function (2) for the second phase of the long swarm. The blue histogram shows the actual distribution of function (2) values for all events relative to their respective "nearest neighbors." The red histogram marks the approximation of the right group of events, and the yellow histogram designates the obtained distribution of clustered events.

The estimation of $k = 0.6$ using the proximity function (2) differs slightly from the original value of $k = 0.64$ (Table 1). For further study, we select an alternative variant, as a case with the most pronounced bimodality of the distribution. Using this procedure, we identify 42 clusters; they are shown in Fig. 4. In each cluster, we define the strongest event, as the main shock, and the events prior to and after it, as foreshocks and aftershocks, respectively. Each cluster contains 37 aftershocks and 58 foreshocks. Table 2 presents the parameters of the independent and clustered events in the second phase of the long swarm. The slope parameter of the magnitude-frequency distribution b, maximum magnitude $M_{\max}$, and the average magnitude $\bar{M}$ are determined.

Table 2. Parameters of independent and clustered events in the second phase of the long swarm

	b	$M_{\max}$	$\bar{M}$
Clustered	0.989	1.5	0.4401
Independent	1.906	1.1	0.2726

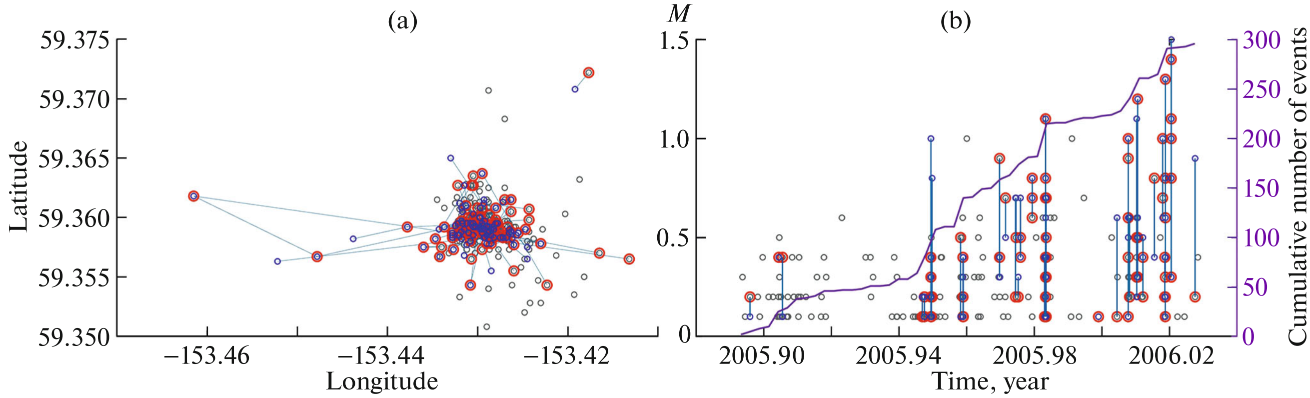

Fig. 4. Clusters of events during the second phase of the long swarm. (a) Space distribution, (b) time distribution. Gray circles indicate independent events (the proximity function values relative to the nearest neighbor exceed the threshold), blue circles mark connected events (the proximity function values are below the threshold); the red outline marks events with "offsprings" (i.e., clustered events), and blue lines denote connections among events within clusters.

DISCUSSION

We analyzed the features of the seismic regime on the three intervals prior to the eruption of Augustine Volcano. The first interval, which is the first phase of the long swarm, is characterized by radial deformations, which can be approximated by a point-source spherical model approximately at the sea level depth [6]. This effect may be caused by increasing pressure in the magma chamber. The second interval, which is the second phase of the long swarm, corresponds to the process of magma dike intrusion [6]. The short swarm is hypothetically related to the final breakthrough of the conduit to the surface [3].

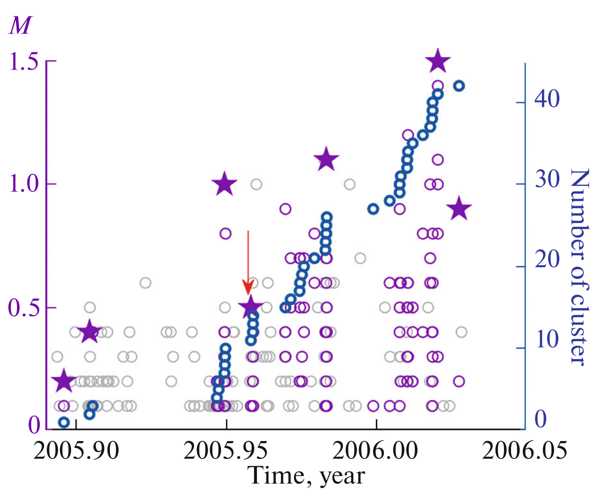

Fig. 5. Time distribution of clusters in the second phase of the long swarm. Blue circles designate the average time positions of events in each cluster, and the values along the vertical line correspond to the sequence number of clusters. Purple circles mark cluster events, and gray circles show the remaining independent events. Purple stars represent the strongest events in cluster sequences. The red arrow depicts a sequence that is inconsistent with the common pattern.

It turned out that the first and third intervals are characterized by a low level of event grouping (Table 1). In contrast, the second interval (the period of dike intrusion) showed a significant degree of event grouping. Here, if only the independent events are considered, the values of the slope parameter of the magnitude–frequency distribution and the average and maximum magnitudes (Table 2) are similar to the values observed during the first phase of the long swarm prior to the onset of the intrusion process (Table 1). This indicates the occurrence of only one process, which is pressure of the spherical source, during the long swarm. This process has a high slope of the magnitude-frequency distribution and relatively low maximum magnitudes, i.e., many small-scale failures occur. The increase in the maximum magnitude during the second phase of the long swarm is likely caused by a different process, dike intrusion, which induces localized destruction of the medium. This process has the slope of the magnitude-frequency distribution close to the "classical" value for tectonic seismicity. This fact also partly explains the significant variations in the *b* parameter observed prior to the eruption: first, pressure increases in the magma chamber leading to an abnormally high *b*-value, then closer to the eruption, the process of intrusion begins, *b*-value decreases, and the degree of clustering increases.

We examined this process in more detail (Fig. 5). It is possible to trace the following tendency: first, a sequence of clusters occurs, terminated by the largest event in the sequence. Then a period of quiescence is observed before the onset of the next sequence of clusters. An exception is only the fourth sequence (marked with a red arrow in Fig. 5), in which the largest event was the first in the sequence.

If we group the clusters into sequences, we obtain a total of 98 foreshocks and 32 aftershocks. Thus, foreshock activity predominates over aftershock activity, which differs from what is usually observed in tectonic seismicity. This could be due to the fact that, in this

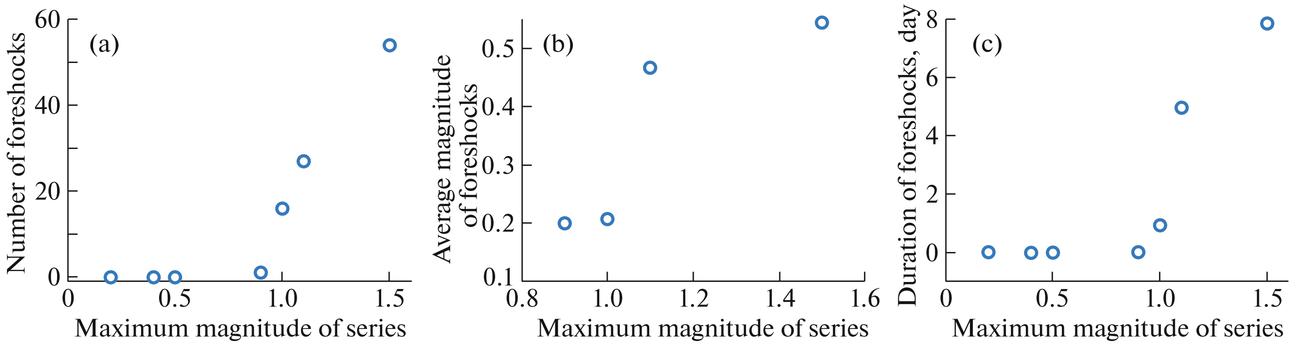

Fig. 6. Dependences on the magnitude of the strongest event in the sequence. (a) Number of foreshocks in the sequence, (b) average magnitude of foreshocks, and (c) duration of the foreshock sequence.

situation, a medium that has not yet been prepared fails under the impact of an intense external source, while the aftershocks are formed depending on the state of the medium and the developed fracture system [18].

We also identify several quality trends:

(1) The larger the magnitude of the main event, the greater the number of foreshocks and the higher their magnitudes (Figs. 6a, 6b).

(2) The larger the magnitude of the main event, the longer the sequence of foreshocks (Fig. 6c).

We suggest one of the possible interpretations. The process of intrusion itself is inhomogeneous: some segments are passed through without resistance; others have "plugs." An obstruction can be removed by sufficient accumulated stress, which depends on the conventional strength of this obstruction (the quiescence between the sequences). When the accumulated stress reaches a certain threshold value, the destruction process begins, occurring gradually rather than instantaneously. This mechanism corresponds, for example, to the avalanche unstable fracturing formation model [19]. The maximum shock magnitude probably depends on the obstruction strength, which affects the duration of the destruction process and the number and strength of foreshocks. The relationship between the number and strength of foreshocks is likely to be trivial and follows from the Gutenberg—Richter law [10]. The relationship with the duration of the process might be characterized by the rate of stress accumulation and the properties of the medium. Some of the described tendencies in foreshock activity have already been described, e.g., in [20].

CONCLUSIONS

The seismicity of Augustine Volcano in Alaska prior to the 2006 eruption was analyzed [4].

Based on the changes in the activity and surface deformations [6], this period covers two processes: first, radial deformation and uplift of the volcanic edifice, then dike intrusion. The initial period is characterized by a high slope parameter of the magnitude—frequency distribution. The phase of intrusion is associated with strong anomalies and time variations in the slope of the magnitude-frequency distribution [4]. Using the nearest neighbor method, time clustering of events in this phase was distinguished. With clusters being removed during the period of intrusion, the seismicity shows a regime similar to that observed during the initial phase of the long swarm. This suggests that this phase continues the seismic activity initiated by radial deformations. The seismicity of the grouped events during the intrusion phase differs significantly (parameter b is close to 1, which is typical of tectonic seismicity). This process is likely to correspond to local destruction of the stress-state medium with the developed system of fractures. The superposition of two processes with different regimes of seismicity also partly explains the observed variations in the parameter b during this period.

The analysis of seismic event clusters shows that the clusters themselves are grouped into sequences. There is a tendency that a sequence of clusters is terminated by the strongest event, followed by a period of quiescence and a new sequence of clusters. This pattern corresponds to a model of earthquake preparation, where stresses accumulate and are released through destruction that starts from a small scale. In this case, the mechanism of stress accumulation is an intense external action, which is the magma pressure. This is likely to cause the predominance of the foreshock activity over the aftershock activity compared to the tectonic seismicity.

FUNDING

This work was carried out as a State Assignment of the Institute of Earthquake Prediction Theory and Mathematical Geophysics, Russian Academy of Sciences.

CONFLICT OF INTEREST

The authors of this work declare that they have no conflicts of interest.

REFERENCES

1. D. Sornette and A. Helmstetter, Phys. A: Statist. Mech. Appl. **318**, 577–591 (2003). https://doi.org/10.1016/S0378-4371(02)01371-7
2. P. Traversa and J.-R. Grasso, Bull. Seismol. Soc. Am. **100** (2010). https://doi.org/10.1785/0120090214
3. H. Buurman and M. E. West, U.S. Geol. Surv. Prof. Paper 1769-2 (2010). https://doi.org/10.3133/pp17692
4. K. Jacobs and S. Mcnutt, U.S. Geol. Surv. Prof. Paper (2010), pp. 59–75.
5. J. A. Power, P. A. Friberg, M. M. Haney, T. Parker, S. D. Stihler, and J. P. Dixon, U.S. Geol. Surv. Sci. Invest. Report. 2019–5037, 2019. https://doi.org/10.3133/sir20195037
6. P. F. Cervelli, T. Fournier, J. Freymueller, J. A. Power, Geophys. Res. Lett. **33**, L18304 (2006). https://doi.org/10.1029/2006GL027219
7. I. Zaliapin, A. Gabrielov, V. I. Keilis-Borok, and H. Wong, Phys. Rev. Lett. **101**, 018501 (2008). https://doi.org/10.1103/PhysRevLett.101.018501
8. I. Zaliapin and Y. Ben-Zion, J. Geophys. Res. Solid Earth **118**, 2847–2864 (2013). https://doi.org/10.1002/jgrb.50179
9. M. Baiesi and M. Paczuski, Statist., Nonlinear, Soft Matter Phys. **69** (066106) (2004). https://doi.org/10.1103/PhysRevE.69.066106
10. B. Gutenberg and C. Richter, Nature **156**, 371–371 (1944).
11. P. N. Shebalin, C. Narteau, and S. V. Baranov, Geophys. J. Int. **222** (2), 1264–1269 (2020). https://doi.org/10.1093/gji/ggaa252
12. S. D. Matochkina, P. N. Shebalin, V. B. Smirnov, A. V. Ponomarev and P. A. Malyutin, Izv., Phys. Solid Earth **60** (5), 913–922 (2024).
13. S. V. Baranov and P. N. Shebalin, *Patterns of Postseismic Processes and Forecast of the Danger of Strong Aftershocks* (Russ. Acad. Sci., Moscow, 2019) [in Russian].
14. A. Mignan and J. Woessner, Estimating the magnitude of completeness for earthquake catalogs, Community Online Resource for Statistical Seismicity Analysis, 2012. https://doi.org/10.5078/corssa-00180805
15. B. Bender, Bull. Seismol. Soc. Am. **73**, 831–851 (1983).
16. P. Grassberger and I. Procaccia, Phys. Rev. Lett. **50** (5), 346–349 (1983).
17. C. Frohlich and S. D. Davis, Geophys. J. Int. **100**, 19–32 (1990).
18. C. Narteau, P. Shebalin, and M. Holschneider, J. Geophys. Res. **107** (B12), 2359 (2002). https://doi.org/10.1029/2002JB001868
19. G. A. Sobolev, Izv., Phys. Solid Earth **55** (1), 138–151 (2019). https://doi.org/10.31857/S0002-333720191166-179
20. A. Helmstetter and D. Sornette, J. Geophys. Res. **108** (B10), 2457 (2003). https://doi.org/10.1029/2003JB002409

Translated by L. Mukhortova